Applied Catalysis B: Environmental 134–135 (2013) 7–18

Contents lists available at SciVerse ScienceDirect

Applied Catalysis B: Environmental

journal homepage: www.elsevier.com/locate/apcatb

Heterogeneous activation of oxone with CoMg/SBA-15 for the degradation of dye Rhodamine B in aqueous solution

Longxing Hu[a,*], Fan Yang[a], Wencong Lu[b], Ying Hao[a], Hang Yuan[a]

[a] School of Environmental and Chemical Engineering, Shanghai University, Shanghai 2000444, PR China
[b] College of Sciences, Shanghai University, Shanghai 200444, PR China

ARTICLE INFO

Article history:
Received 3 September 2012
Received in revised form
29 November 2012
Accepted 13 December 2012
Available online 3 January 2013

Keywords:
Heterogeneous Co catalysts
Magnesium modified catalysts
Sulphate radicals
Rhodamine B degradation
Oxone activation

ABSTRACT

A novel heterogeneous Co catalyst CoMg/SBA-15 was prepared through a two-step incipient wetness impregnation of Mg and Co into mesoporous silica SBA-15 and used for the activation of oxone to generate sulphate radicals for degrading Rhodamine B (RhB) in aqueous solution. The CoMg/SBA-15 was characterized by several techniques such as XRD, N_2 adsorption–desorption, CO_2-TPD, TEM and SEM. It was found that the CoMg/SBA-15 existed as agglomerates with the particle size more than 0.3 μm, and Co and Mg occurred mainly both inside and outside the support pores in the form of cubic spinel Co_3O_4 and Mg oxide crystallites, respectively. Loading Mg into the support increased the dispersion of Co_3O_4 on the support and generated the remarkable basicity of the catalyst surface promoting the formation of surface Co–OH complex. The CoMg/SBA-15 still displayed the long-range ordered arrangement of the channels in structure with the reduced pore diameter and surface area compared with the SBA-15. The Co/SBA-15–oxone–RhB system, as a test control, was demonstrated to be efficient for the activation of oxone producing sulphate radicals for the degradation of RhB in solution. And the increase of Co/SBA-15 and oxone dosages had the positive effect on the degradation efficiency and rate, with the almost complete RhB degradation in 60 min and the Co leaching concentration less than 43 μg/L and the leaching percent less than 0.40% at appropriate Co/SBA-15 and oxone dosages. In addition, the degradation followed the first-order kinetics. The CoMg/SBA-15 exhibited much higher activity than Co/SBA-15 and Co/MgO with the same Co loading in degrading RhB by sulphate radicals from oxone, with nearly 100% degradation in 5 min, the Co leaching concentration of 80 μg/L and the leaching percent of 0.96%, and almost 100% TOC removal under appropriate conditions achieved. The CoMg/SBA-15 also displayed stable performance during 25 runs of reuse. Based on the UV–vis spectra and TOC measurement, the degradation mechanism of RhB in the presence of CoMg/SBA-15 and oxone was proposed. It is believed that CoMg/SBA-15 can be widely applied in the catalytic oxidation with oxone for the degradation of the refractory organic pollutants such as dye RhB in water.

1. Introduction

Advanced oxidation processes (AOPs), as one of the innovative water and wastewater treatment technologies, are based on the in situ generation of highly reactive radicals, such as hydroxyl radical ($OH^•$), $O_2^{•-}$, $OOH^•$ and sulphate radical ($SO_4^{•-}$), for mineralization of refractory organic pollutants [1–5]. Over the past years, sulphate radicals based-advanced oxidation processes (SR-AOPs) have attracted great interest in the environmental applications because at neutral pH, $SO_4^{•-}$ is a more powerful oxidant for the decomposition of contaminants, and is more selective for oxidation, overcoming some limitations of the conventional Fenton processes [3,6–8]. The coupling of transition ions with oxone or peroxymonosulphate (PMS) for the generation of sulphate radicals to degrade the organic pollutants has been proven to be a highly efficient approach [3,7–9], with cobalt ions being the best activator [8]. However, the adverse effect of dissolved cobalt in water on animals and human beings is always a great concern, leading to a strong desire to develop heterogeneous cobalt catalysts.

So far, several heterogeneous cobalt-based catalysts coupled with oxone for the environmental applications have been investigated, i.e. unsupported cobalt oxides including Co_3O_4 [5,10,11] and CoO [10], unsupported cobalt composites such as iron–cobalt mixed oxide nanocomposite [12,13], supported cobalt catalysts including oxide supported Co catalysts such as TiO_2-, Al_2O_3-, SiO_2-, MgO-, ZnO-, ZrO_2-supported cobalt catalysts [14–18], carbon material supported Co catalysts such as Co/activated carbon [19], Co/carbon-aerogel [20], Co/carbon-xerogel [21] and

* Corresponding author. Tel.: +86 21 6613 7771; fax: +86 21 6613 7771.
E-mail address: hulxhhhb@yahoo.com.cn (L. Hu).

0926-3373/$ – see front matter © 2012 Elsevier B.V. All rights reserved.
http://dx.doi.org/10.1016/j.apcatb.2012.12.028

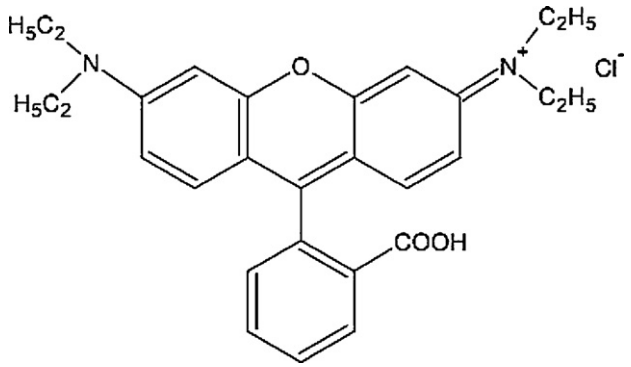

Fig. 1. Molecular structure of Rhodamine B.

Co_3O_4 or $CoFe_2O_4$/graphene oxide [22–24], cobalt exchanged zeolites [25,26], cobalt exchanged resin [26], industrial solid waste supported Co catalysts such as Co/red mud and Co/fly ash [27], and mesoporous material supported Co catalysts such as Co/mesoporous silica SBA-15 [28–30]. For the heterogeneous cobalt catalysts, two requirements should be attained: (1) high catalytic activity and stability including the cobalt leaching in the solution and the recycling performance; (2) convenient recovery of the catalysts after application for water and wastewater treatment [12]. Therefore, as to all the investigated heterogeneous cobalt catalysts, the further enhancement could also be desired to a varying degree, and the development of novel heterogeneous cobalt catalysts for the environmental application is also of great significance.

Mesoporous silica SBA-15, one of mesoporous molecular sieves, has the highly ordered structure, large pore size and high surface area [31,32], which favors the loading and dispersion of the catalytic active component thus enhancing the activity and stability of catalysts. In our previous investigation [28], the Co supported SBA-15 has been proven to be effective in degradation of phenol in water with stable performance. Shukla et al. also reported the same investigation achieving the similar results [29]. However, Co/SBA-15, as a representative potential excellent heterogeneous catalyst for oxone activation to decompose refractory organic pollutants, is still worth further investigation.

RhB, having the molecular structure shown in Fig. 1 and the maximum absorption at 552 nm, is an important water-soluble xanthene organic dye, which is widely used in varying industries resulting in the dye effluents with various concentrations. The RhB in water even at low concentrations interferes with penetration of sunlight into water and the gas solubility in water, retards photosynthesis, inhibits the growth of aquatic biota, and is a suspected carcinogen. The complex structure and stable properties of RhB make it resistant to biological degradation and photodegradation. The major techniques employed to remove RhB from water include adsorption [33,34], photocatalytic oxidation [35,36], Fenton process [37], ultrasonic degradation [38,39], ozonation [40] and electrochemical oxidation [41,42], etc. Adsorption is easy to operate with high removal efficiency, but it only transfers the pollutants from liquid phase to solid phase leading to the secondary pollution. The techniques such as photocatalytic oxidation, ultrasonic degradation, ozonation and electrochemical oxidation require special equipment and devices, resulting in the high capital and operation costs. Fenton process is a rapid and inexpensive process, but it has several significant drawbacks such as the acidic pH requirement (pH 2–4), a high Fe dosage producing a large amount of iron sludge and the TOC removal less than 60%.

In this study, we first explored the feasibility of using Co/SBA-15 to activate oxone for the generation of sulphate radicals followed by the degradation of the refractory organic dye RhB in dilute solution, and then modified the Co/SBA-15 by loading Mg oxide on the support for the improved physicochemical properties and catalytic performance of the resultant catalyst CoMg/SBA-15.

2. Experimental

2.1. Preparation of SBA-15, Co/SBA-15, CoMg/SBA-15 and Co/MgO

SBA-15 was prepared according to the procedure described by Zhao et al. [31]. The catalyst Co/SBA-15 or 10Co/SBA-15, having the fixed Co loading of 10 wt.% in this study, was prepared by incipient wetness impregnation with an aqueous solution of $Co(NO_3)_2{\cdot}6H_2O$ (SCRC) [28]. The impregnated solids were dried at 100 °C for 10 h. Then the dried solids were calcined at 400 °C for 5 h in air. A heating rate of 10 °C/min was used. The catalyst CoMg/SBA-15 was prepared by two-step incipient wetness impregnation using $Co(NO_3)_2{\cdot}6H_2O$ and $Mg(NO_3)_2{\cdot}6H_2O$ as the precursors, respectively, with cobalt loading of 10 wt.% and magnesium loading of 5 wt.%, 10 wt.%, 15 wt.% and 20 wt.%, respectively. A typical synthesis is as follows: Mg/SBA-15 was first prepared by incipient wetness impregnation using $Mg(NO_3)_2{\cdot}6H_2O$ (SCRC) as the precursor and SBA-15 as the support and by the procedures similar to those of Co/SBA-15 synthesis, and CoMg/SBA-15 was then prepared by incipient wetness impregnation using $Co(NO_3)_2{\cdot}6H_2O$ as the precursor, Mg/SBA-15 as the support and by other procedures like the described above. The resulting catalysts were denoted as 10ConMg/SBA-15, where 10 represents 10 wt.%, the loading of Co, and *n* represents *n*wt.%, the loading of Mg. The catalyst Co/MgO was prepared by incipient wetness impregnation using MgO as the support and $Co(NO_3)_2{\cdot}6H_2O$ as the precursor, followed by drying at 60 °C overnight and subsequent calcination at 400 °C for 3 h in static air, which is similar to the procedure described by Zhang et al. [16].

2.2. Characterization of prepared CoMg/SBA-15

XRD patterns of all the samples prepared were obtained on a Rigaku D/Max-2200X powder X-ray diffractometer using Cu Kα radiation source of wavelength 1.54056 Å at 40 kV and 40 mA. The small-angle data were collected from 0.5° to 5.0° (2θ) with a scan speed of 0.5°/min; the wide-angle data were collected from 10° to 80° (2θ) with a scan speed of 5°/min. The mean crystallite size of the cobalt oxide particles was estimated by the Debye–Scherrer equation using profile fitting method for the determination of the full width at half-maximum (FWHM) of Co_3O_4 (3 1 1) reflections. N_2 adsorption–desorption isotherms were measured using Micromeritics Tristar 3000 at 77 K. The specific surface areas were evaluated using Brunauer–Emmett–Teller (BET) method in the p/p_0 range of 0.02–0.20. The pore size distributions were calculated using the Barrett–Joyner–Halenda (BJH) method based on the adsorption branch. The total pore volume was determined from the date at $p/p_0 = 0.99$. The internal structure of the sample prepared was characterized by a JEM-2010F (JEOL) high resolution-transmission electron microscope (HRTEM) with field emission gun at 200 kV. The external morphology of the sample was observed on a JSM-6700F scanning electron microscope (SEM). The basicity of the samples was measured with a chemisorptive analyzer CHEBET 3000.

2.3. RhB degradation in the presence of Co/SBA-15 or CoMg/SBA-15-oxone

In this investigation, the performance of the catalyst refers to the catalytic activity and stability, with the catalytic activity and stability represented by the decolourization efficiency and rate of dye RhB, and cobalt and magnesium leachings in aqueous solution, respectively. The Co or Mg leaching, was represented

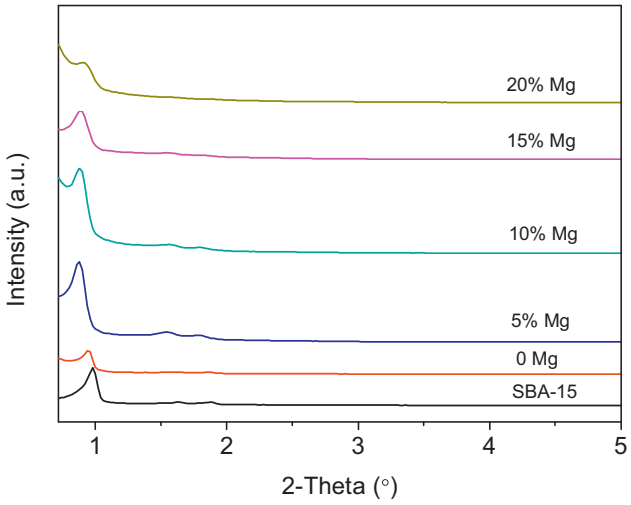

Fig. 2. Low-angle XRD patterns of SBA-15 and CoMg/SBA-15 with various Mg loadings.

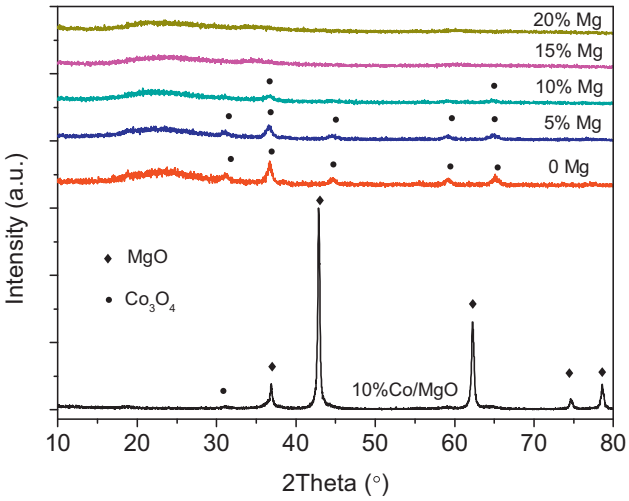

Fig. 3. Wide-angle XRD patterns of 10Co/MgO and CoMg/SBA-15 with various Mg loadings.

by leaching concentration (dissolved Co or Mg concentration in solution) and leaching percent (% loss of Co or Mg into the solution), respectively. The batch degradation experiments were carried out at ambient temperature (~25 °C) in 1 L reactor with 500 mL of RhB (SCRC) solution (5.0 mg/L unless otherwise stated) which were placed on a magnetic stirrer plate. The initial pH of the solution was not adjusted. A known amount of oxidant, oxone ($2KHSO_5$ $KHSO_4{\cdot}K_2SO_4$, $KHSO_5$ (PMS) as active component, Shanghai Future Chemical Technology Co., Ltd.) was added to the RhB solution and allowed to completely dissolve with the oxone/RhB molar ratio fixed at 5:1–50:1, and then a given amount of the catalyst was added into the reactor to start the reaction with catalyst dosage ranging from 0.02 g/L to 0.25 g/L. The reactor was covered to avoid volatilization. At fixed reaction time intervals, reaction mixture samples (about 5 mL for each) were withdrawn from the suspension and then filtered. At the end of reaction, samples were quenched with excess sodium nitrite to prevent further reaction and filtered with filter paper prior to analysis. The RhB concentrations in aqueous solution were determined by means of UV–vis spectrophotometry (UV-5300PC) at 552 nm and the UV–vis absorption spectra of the selected RhB aqueous solutions were recorded. Cobalt ion concentration in solution was measured by nitroso-R-salt spectrophotometric method using a 722E visible spectrophotometer at 425 nm. The magnesium in solution was measured by an inductively coupled plasma (ICP) emission spectrometer (Prodigy). The total organic carbon (TOC) of the selected samples was measured by Shimadzu TOC-5000A analyzer. For the recycle test of the catalyst, after each run, the spent catalyst CoMg/SBA-15 was filtered from the reaction mixture with filter paper, and then all the materials were dried and calcined at 400 °C for 3 h to get the filter paper ashed and a recyclable catalyst produced. Several parallel reactions were carried out in every run before the last run to ensure the catalyst amount was enough for the next run. Generally, the experiments were conducted in duplicate and the errors of the experimental results were below 3%.

3. Results and discussion

3.1. Characterization of CoMg/SBA-15

3.1.1. XRD

The small angle XRD spectra of prepared SBA-15 and CoMg/SBA-15 with different magnesium loadings are depicted in Fig. 2. The SBA-15 exhibited three well-resolved diffraction peaks at 0.982, 1.640 and 1.882 of 2θ, which were indexed as the (1 0 0), (1 1 0) and (2 0 0) reflections associated with the p6mm hexagonal symmetry. For 10 wt.%Co/SBA-15, the reflection intensity decreased appreciably, indicating the effect of the cobalt oxides supported on the support. For the 10Co5Mg/SBA-15, there were a diffraction peak at 0.982 of 2θ, corresponding to (1 0 0) reflection, and stronger diffraction peaks corresponding to (1 1 0), (2 0 0) reflections than those for the 10 wt.%Co/SBA15, suggesting that the Mg loading on the SBA-15 could result in the increased cobalt oxide particle dispersion on support, reducing the effect of cobalt oxides on the XRD of SBA-15. However, the decrease in intensity of the diffraction peaks in CoMg/SBA-15 with increasing Mg incorporation could be attributed to the decrease in electron density contrast due to the increased Mg loading [43].

Fig. 3 shows the wide-angle XRD spectra of synthesized 10Co/MgO and CoMg/SBA-15 with various Mg loadings. The 10Co/MgO displayed a high-intensity peak of MgO, but no distinct diffraction peak of Co_3O_4 phase, which was also reported in the literature [16]. The reasons may be that the loading of Co in Co/MgO was not high enough and the weak diffraction peaks of Co_3O_4 phase were masked by the strong diffraction peaks of MgO. As observed, the characteristic diffraction peaks of Co_3O_4 occurred in CoMg/SBA-15, but their intensity of reflections decreased with the increase of the Mg loading, indicating that Co_3O_4 particles were better dispersed on SBA-15 arising from the increased Mg introduction. No distinct diffraction peaks of MgO were observed in samples of 10Co5Mg/SBA-15, 10Co10Mg/SBA-15, 10Co15Mg/SBA-15 and 10Co20Mg/SBA-15, implying that MgO had high dispersion on the support SBA-15 without the formation of large crystallites.

3.1.2. N_2 adsorption–desorption

The nitrogen adsorption–desorption isotherms of SBA-15, fresh 10Co10Mg/SBA-15, spent 10Co10Mg/SBA-15 and regenerated 10Co10Mg/SBA-15 are depicted in Fig. 4. All the samples exhibited type IV isotherms with a H1-type hysteresis loop resulting from the capillary condensation of nitrogen in the mesopores, which was characteristic of mesoporous materials having cylindrical type mesostructures. The isotherm of the SBA-15 displayed a sharp jump at a relative pressure of 0.6–0.8, indicating that the sample had the typical mesostructure with uniform pore size distribution. But isotherms of the fresh, spent and regenerated 10Co10Mg/SBA-15 samples exhibited a sharp jump at a relative pressure of 0.4–0.8 lower than that for the SBA-15, indicating that the pore size of the support SBA-15 decreased after the loading of

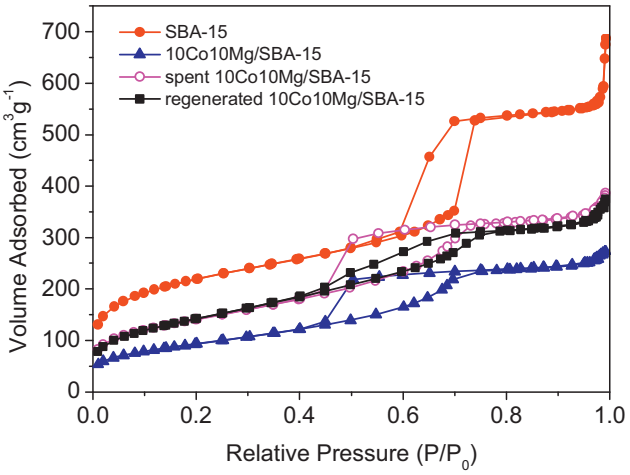

Fig. 4. N_2 adsorption–desorption isotherms of SBA-15, fresh 10Co10Mg/SBA-15, spent 10Co10Mg/SBA-15 and 10Co10Mg/SBA-15 regenerated by calcination.

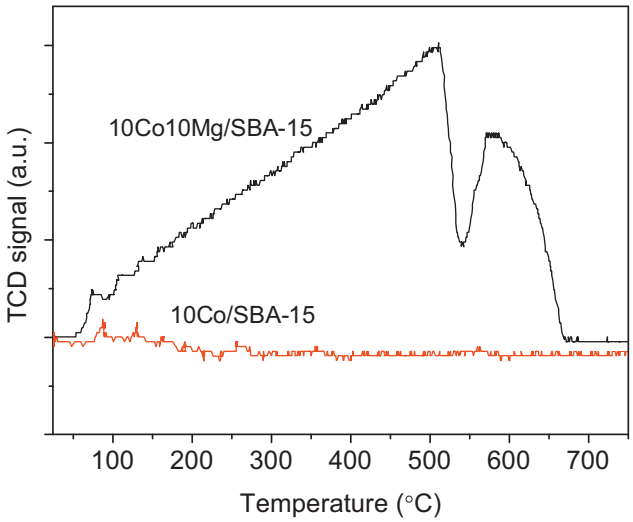

Fig. 5. CO_2-TPD patterns of 10Co/SBA-15 and 10Co10Mg/SBA-15.

Co and Mg species and the supported species indeed entered into the channels of the SBA-15. For all 10Co10Mg/SBA-15 samples, the jumps on the isotherms were less sharp, suggesting that to a certain degree the uniform pore size distribution of the support SBA-15 was lost after the Co and Mg loading.

The pore parameters of the investigated catalysts are listed in Table 1. Because cobalt and magnesium oxides formed by calcination occupied the pore space of SBA-15, the introduction of Co and Mg led to a significant decrease in the specific surface area, pore volume and pore size of the materials (Table 1). As seen, for the spent catalyst 10Co10Mg/SBA-15, a further slight decrease of pore size and increases of the specific surface area and pore volume were observed, which could be due to the high amount of Mg leaching during the reaction. In our investigation, it was noticed that after the first utilization of the catalyst 10Co10Mg/SBA-15, the maximum Mg leaching of 4 mg/L would appear in the aqueous solution, meaning that some supported magnesium species dissociated from solid catalyst and dissolved in the solution, resulting in the increased specific surface area and pore volume. Compared with the spent catalyst, the catalyst 10Co10Mg/SBA-15 regenerated by calcination possessed the slightly increased specific surface area, slightly reduced pore volume and pore size (Table 1), which might be ascribed to the shrink, collapse and destruction of the support channels due to the high-temperature calcination.

3.1.3. CO_2-TPD

The CO_2 temperature programmed desorption (CO_2-TPD) experiments were performed to characterize the surface basic sites of the catalyst samples. The strength and amount of the basic sites were reflected by the desorption temperature and the peak area, respectively, in a CO_2-TPD profile. Fig. 5 shows the CO_2-TPD profiles of 10Co/SBA-15 and 10Co10Mg/SBA-15. At 50–150 °C, both catalysts showed two weak CO_2 uptake peaks, which was closely related to the physicosorption of the CO_2 molecules on the surface of the catalysts. At higher temperatures, there were no obvious CO_2 desorption peaks in the CO_2-TPD pattern of 10Co/SBA-15, with the original weak acidity of SBA-15 surface remaining unchanged on the surface of the catalyst Co/SBA-15. However, at 400–700 °C of CO_2-TPD profile, the catalyst 10Co10Mg/SBA-15 exhibited two CO_2 desorption peaks of high intensity, indicating that the strong basic sites occurred on the surface of 10Co10Mg/SBA-15.

Table 1
Pore parameters of SBA-15, fresh 10Co10Mg/SBA-15, spent 10Co10Mg/SBA-15 and 10Co10Mg/SBA-15 regenerated by calcination.

Sample	BET surface area ($m^2\ g^{-1}$)	Pore volume ($cm^3\ g^{-1}$)	Pore diameter[a] (nm)
SBA-15	784.6	1.062	6.9
10Co10Mg/SBA-15	334.5	0.422	5.0
Spent 10Co10Mg/SBA-15	505.4	0.598	4.7
Regenerated 10Co10Mg/SBA-15	511.6	0.579	4.5

[a] Calculated from the adsorption branch of the isotherm.

3.1.4. TEM

The HRTEM images of the synthesized 10Co10Mg/SBA-15 are presented in Fig. 6. A highly ordered array was observed, which was an indication for the preservation of the long-range ordered arrangement of the channels in SBA-15 loaded with cobalt and magnesium (Fig. 6). The places with darker contrast in Fig. 6(a) and (c) could be assigned to the presence of metal oxide particles which located into the SBA-15 channels and occurred as small crystallites resulting from calcination. This was also confirmed clearly in Fig. 6(b), where the bright spots could be ascribed to the supported cobalt and magnesium oxide crystallites. The growth of these crystallites embedded into the mesostructured support was controlled by the mesoporous silica walls, with the rodlike crystallites formed after calcination. The diameters of these crystallites were 6.6 nm comparable to the pore diameter of SBA-15, while the length of the crystallites was more than 10 nm, which could be ascribed to their non-limited growth along the channel direction. Based on the analysis of EDS, the dark area circled in Fig. 6(d) represented the mixed metal oxide crystallites, which confirmed that Co and Mg species indeed located into the support channels, consistent with the results of N_2 adsorption–desorption.

3.1.5. SEM

Fig. 7 presents the SEM images of the SBA-15, fresh 10Co10Mg/SBA-15 and spent 10Co10Mg/SBA-15. As observed, all the samples appeared in the form of aggregates with the diameters more than 0.3 μm. Comparing Fig. 7(a) with (b), it is found that there were more attached small particles on the surface of the catalyst 10Co10Mg/SBA-15, indicating that some cobalt and magnesium oxides agglomerated on the external surface of the catalyst forming larger particles. For the spent catalyst, many small particles were still observed on the surface of the catalyst (Fig. 7(c)), indicating the firm connection of the small particles with the support.

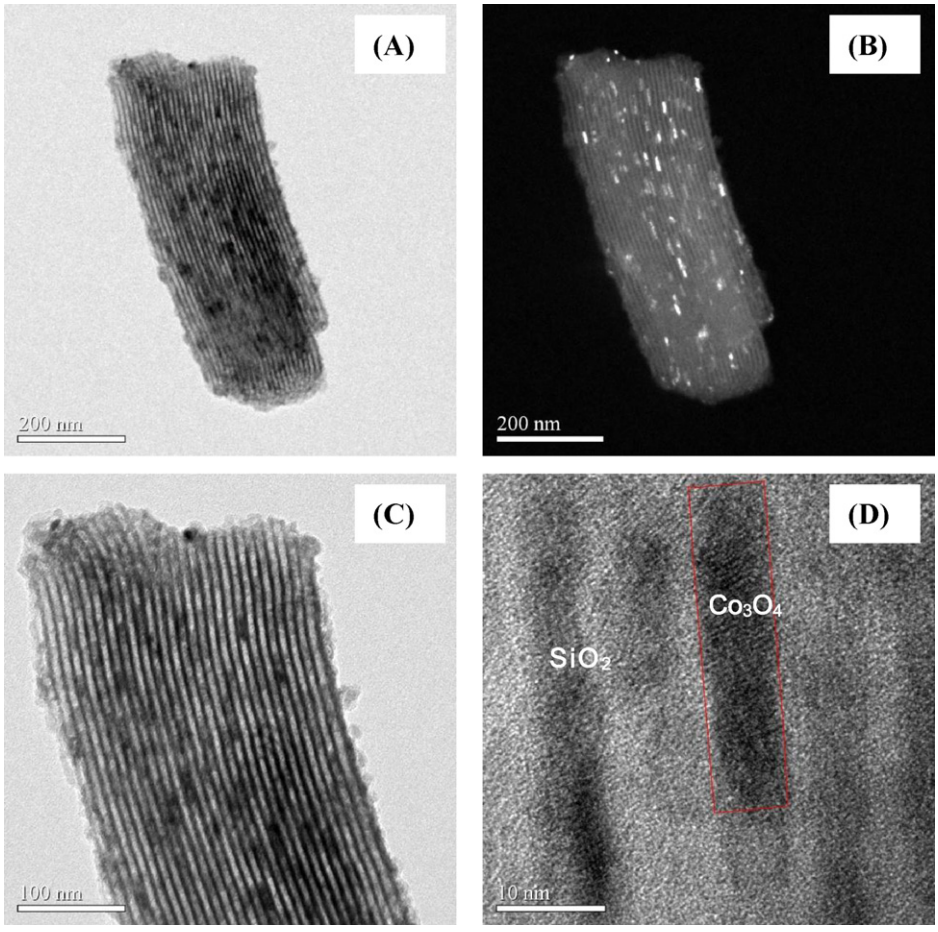

Fig. 6. HRTEM images of 10Co10Mg/SBA-15 (bright field: (a)–(c); and dark field: (d)).

3.2. RhB degradation in the presence of Co/SBA-15 and oxone

In our previous investigation [28], the Co/SBA-15 has been proven to be an easily recyclable and efficient catalyst for heterogeneous activation of oxone for the degradation of phenol in water, so it was expected to be still efficient for the catalytic degradation of the refractory organic dye RhB in aqueous solution. Moreover, as control experiments for CoMg/SBA-15-oxone test, the degradation of RhB in the Co/SBA-15 and oxone system was carried out to present some instructive information. The effects of important parameters such as Co/SBA-15 dosage and oxone dosage on RhB degradation are presented as follows.

3.2.1. Effect of Co/SBA-15 dosage on catalyst performance

In the Co/SBA-15–oxone–RhB system, the Co/SBA-15 was used as the catalyst for the activation of oxone to generate the active radicals, and the RhB was the target compound of the radical attack. Thus, the generation of sulphate radicals can be affected by the concentrations of catalyst and oxone. In this heterogeneous system, the reaction efficiency and rate was generally controlled by the generation of the radicals, thus by the concentrations of Co/SBA-15 and oxone. Because of the crucial role of the catalyst for RhB degradation with oxone, the kinetic study on Co/SBA-15 was first conducted. Fig. 8(a) shows RhB degradation on Co/SBA-15 with oxone at various catalyst loadings, i.e. the normalized RhB concentration profiles

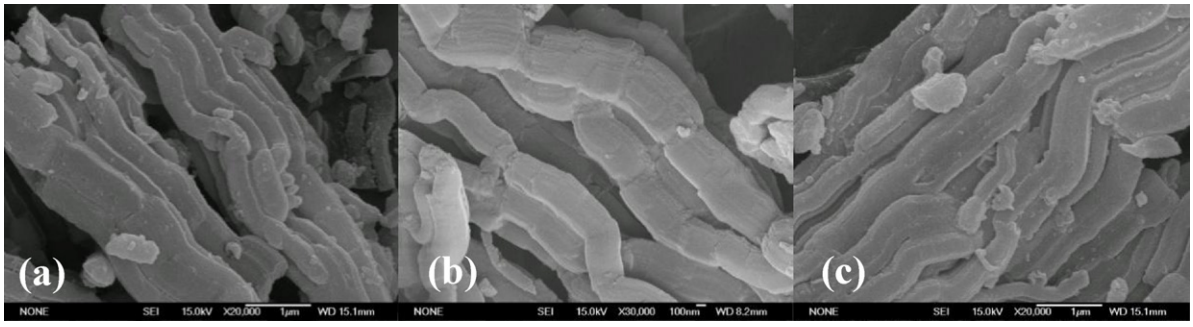

Fig. 7. SEM images of SBA-15 (a), fresh 10Co10Mg/SBA-15 (b) and spent 10Co10Mg/SBA-15(c).

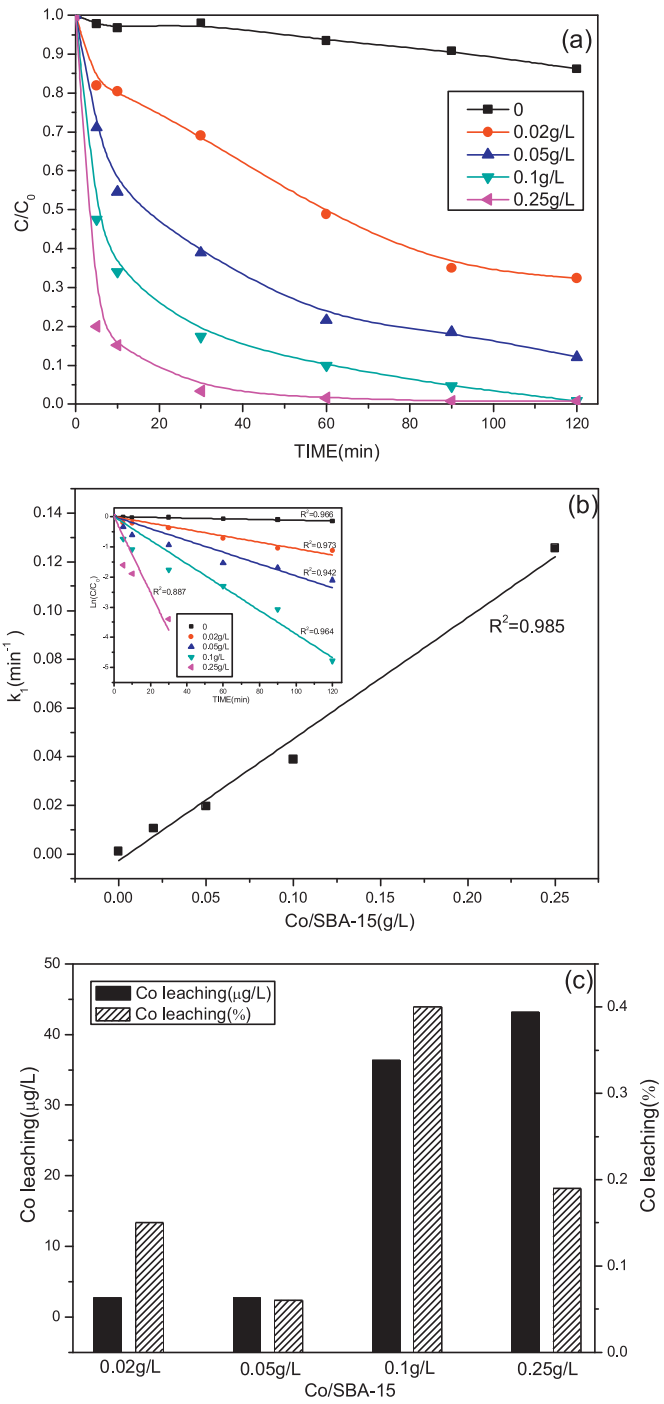

Fig. 8. Performance of catalyst Co/SBA-15 at various Co/SBA-15 dosages in the presence of oxone and RhB ((a) RhB degradation, (b) RhB degradation kinetics, and (c) cobalt leaching. C_{RhB}: 5.0 mg/L, Co/SBA-15 dosage: 0 g/L, 0.02 g/L, 0.05 g/L, 0.10 g/L, 0.25 g/L, molar ratio of oxone/RhB: 10:1, T: 25 °C, reaction time: 2 h, and no solution pH adjustment).

at varying catalyst dosages with oxone. Higher Co/SBA-15 loading in solution resulted in higher RhB degradation efficiency and rate (Fig. 8(a) and (b)). At 0.02 g/L of Co/SBA-15, RhB degradation only reached 65% in 120 min, while it could reach almost 100% in 60 min at 0.25 g/L loading of Co/SBA-15. The enhanced dosage of the catalyst would increase adsorption sites and also provide more catalytic active sites for activation of oxone to generate more sulphate radicals, and thus would lead to a significant enhancement of the reaction rate. Fig. 8(b) illustrates that the RhB degradation followed well the first-order kinetic model $\ln C/C_0 = -k_1 t$, where C and C_0 are the RhB concentration at time (t) and $t = 0$, respectively, and k_1 is the rate constant, and that the rate constant k_1 increased linearly with increasing catalyst dosage. In addition, it is noteworthy that for the reaction taking place in the presence of oxone alone, a change of less than 15% in RhB concentration was found at 120 min, confirming that the oxone itself in homogeneous solution could not induce significant RhB degradation.

Fig. 8(c) presents the Co leaching at various catalyst dosages in the system of Co/SBA-15 coupled with oxone and RhB. It was observed that the Co leaching concentration increased essentially with increased Co/SBA-15 dosage, with 43 μg/L of Co leaching concentration at the highest dosage of 0.25 g/L, while the Co leaching percent remained at the low level of 0.06–0.40%. Based on the degradation efficiency and rate as well as the Co leaching, it could be believed that the optimal catalyst dosage ranged from 0.10 to 0.25 g/L under other fixed reaction parameters.

3.2.2. *Effect of oxone dosage on performance of catalyst Co/SBA-15*

Fig. 9(a) shows RhB degradation at various oxone dosages (in terms of molar ratio of oxone/RhB) in the presence of Co/SBA-15, i.e. the normalized RhB concentration profiles at varying oxone dosages with Co/SBA-15. Fig. 9(b) presents the corresponding relationship between initial reaction rate constant and oxone dosage, with the inset figure showing the kinetic fitting curve. From Fig. 9(a) and (b), it is found that the higher the molar ratio of oxone/RhB, the faster the RhB degradation rate and the higher the degradation efficiency at the appropriate catalyst dosage. The RhB degradation could reach 100% as the molar ratio of oxone/RhB exceeded 10:1, with the colour of the RhB solution disappearing completely. As shown in Fig. 9(b), RhB degradation also follows the first-order kinetics with respect to RhB, with the reaction rate k_1 increasing significantly with oxone dosage. It was reported that the further increase in oxone dosage would result in lower degradation efficiency and rate for the organic compounds in the system of cobalt-based catalyst and oxone due to the self-quenching of sulphate radicals by PMS (oxone)[29]. However, the negative effect of the higher oxone dosages on RhB degradation efficiency and rate was not observed in this case probably due to the harmonious proportion among the catalyst, oxidant and target compound. Because the initial RhB concentrations of the solution investigated were as low as 5.0 mg/L for simulating the dilute wastewater effluent, the kinetic models were related to the concentration of the reactant RhB which became one of the rate-limiting factors. Moreover, the RhB degradation reached a maximum of approximately 35% at 10 min of reaction in the presence of Co/SBA-15 without oxone, which was attributed to the adsorption capability of Co/SBA-15 due to its mesoporous structure. In the case of the co-existence of catalyst and oxone, considering the separate contributions of the adsorption by catalyst (Fig. 9(a)) and oxidation by oxone alone (Fig. 8(a)), the degradation behavior could be predominantly ascribed to the fast catalytic oxidization by sulphate radicals rather than the adsorption. The Co leaching at various oxone dosages in the presence of Co/SBA-15 and RhB is shown in Fig. 9(c). The Co leaching concentration and percent ranged from 20 to 39 μg/L and from 0.22 to 0.43%, respectively, and the cobalt leaching difference arising from the various oxone dosage was insignificant. It was experimentally found that the initial pH of the solutions with the various oxone dosage ranged from 3.0 to 4.5, thus the proximity of the pH would not lead to the remarkable cobalt leaching difference.

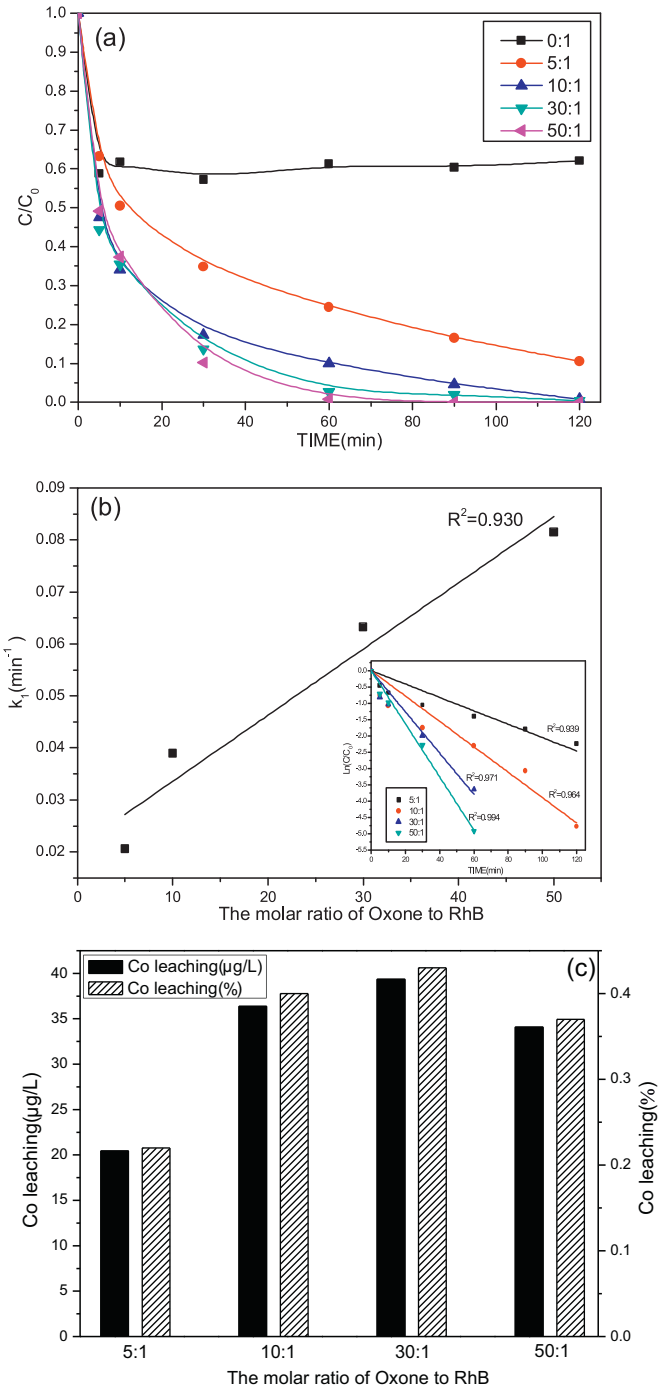

Fig. 9. Performance of catalyst Co/SBA-15 at various oxone dosages in the presence of Co/SBA-15 and RhB ((a) RhB degradation, (b) RhB degradation kinetics, (c) cobalt leaching, C_{RhB}: 5.0 mg/L, Co/SBA-15 dosage: 0.10 g/L, molar ratio of oxone/RhB: 0:1, 5:1, 10:1, 30:1, 50:1, *T*: 25 °C, reaction time: 2 h, and no solution pH adjustment).

3.3. RhB degradation in the presence of CoMg/SBA-15 and oxone

It was demonstrated that RhB could be degraded efficiently in the Co/SBA-15–oxone system (Section 3.2). Besides, in the previous study [16] on heterogeneous activation of oxone with supported cobalt oxide on MgO for degradation of organic dyes in dilute solutions, it was suggested that the surface basic sites on the MgO support could promote the formation of the surface Co–OH complex which is a critical step for activation of oxone during the reaction. Also, in the investigation of Yang et al. [12], the authors reported a novel approach of using Fe–Co mixed oxide nanocatalysts for the heterogeneous activation of oxone to generate sulphate radicals for decomposition of an organic pollutant with a suggestion that the presence of Fe was beneficial for enriching hydroxyl group content on the Fe–Co catalyst surface, which can facilitate the formation of Co(II)–OH complexes that are vital for oxone activation. Furthermore, it was reported that increasing the basicity of the support favored the reduction of the carbon deposit on the catalyst surface [44,45], and the extension of catalyst service life. Therefore, the modification of the catalyst Co/SBA-15 by loading appropriate amount of magnesium into it to increase the basicity of catalyst surface was made, and the subsequent application of the catalyst for degrading RhB in the presence of oxone was explored.

3.3.1. Performance of cobalt-based heterogeneous catalysts with various supports and homogeneous Co(II) catalysts

Fig. 10(a) shows RhB degradation in the system of Co-loaded heterogeneous catalysts with different supports and oxone, and Fig. 10(b) displays RhB degradation kinetics in the same systems. The three different supports investigated were 10 wt.%Mg/SBA-15, SBA-15 and MgO, respectively, and the corresponding catalysts were designated as 10Co10Mg/SBA-15, 10Co/SBA-15 and 10Co/MgO, respectively. From Fig. 10(a) and (b), it is observed that the three catalysts with the same cobalt loading display distinctly different catalytic activity, represented by RhB degradation efficiency and rate. The catalytic activity followed the order: 10Co10Mg/SBA-15 > 10Co/SBA-15 > 10Co/MgO, with remarkable difference between any two activities. RhB was degraded very fast under the influence of 10Co10Mg/SBA-15 and oxone. The complete decolourization of the RhB could be achieved in 5 min for 10Co10Mg/SBA-15–oxone, while about 87% decolourization in 60 min for 10Co/SBA-15–oxone, and only 52% of RhB decolourization in 60 min with 10Co/MgO and oxone. The loading of an appropriate amount of Mg oxide on support SBA-15 makes the slightly acidic surface of the support become slightly basic, which was confirmed by the CO_2-TPD test (Section 3.1.3). The basic sites of the support surface can facilitate the formation of the surface Co–OH complex, which is crucial to activating oxone [12,16]. Hence, a much better catalytic activity of 10Co10Mg/SBA-15 compared with Co/SBA-15 was ascribed to the desirable basic sites on the surface of the Mg modified SBA-15. Moreover, 10Co10Mg/SBA-15 had better catalytic activity than 10Co/MgO could also be explained as follows: except for the common feature of the basic surface for the two catalysts, 10Co10Mg/SBA-15 possesses the mesoporous structure resulting in high surface area, large pore volume and more uniform pore size, which could cause the uniform dispersion of nano cobalt oxides, leading to the nano effect of the catalyst.

Fig. 10(b) illustrates that data fitting of the first-order kinetics was very well for the three cobalt-based catalysts with different supports, and the k_1 values have the substantial value for the differentiation of the degradation rates on three catalysts. The rate constant k_1 for 10Co10Mg/SBA-15 was shown to be much higher than those for the other two catalysts (Fig. 10(b)), indicating a very fast generation of free sulphate radicals once oxone is in contact with the catalyst 10Co10Mg/SBA-15. Plenty of sulphate radicals were responsible for the rapid RhB degradation in the initial several minutes.

Fig. 10(c) presents Co and Mg leachings under the effects of three different cobalt-based heterogeneous catalysts coupled with oxone and RhB. 10Co10Mg/SBA-15 had the moderate and acceptable Co leaching among the three different catalysts, which make it very promising for the application. It was observed that Co leachings for 10Co10Mg/SBA-15, 10Co/SBA-15 and 10Co/MgO after 60 min of reaction reached 80 μg/L (0.96%), 36 μg/L (0.40%) and 130 μg/L (1.44%), respectively, and Mg leaching concentration for 10Co10Mg/SBA-15 was equivalent to 4.3 mg/L less than 10.4 mg/L

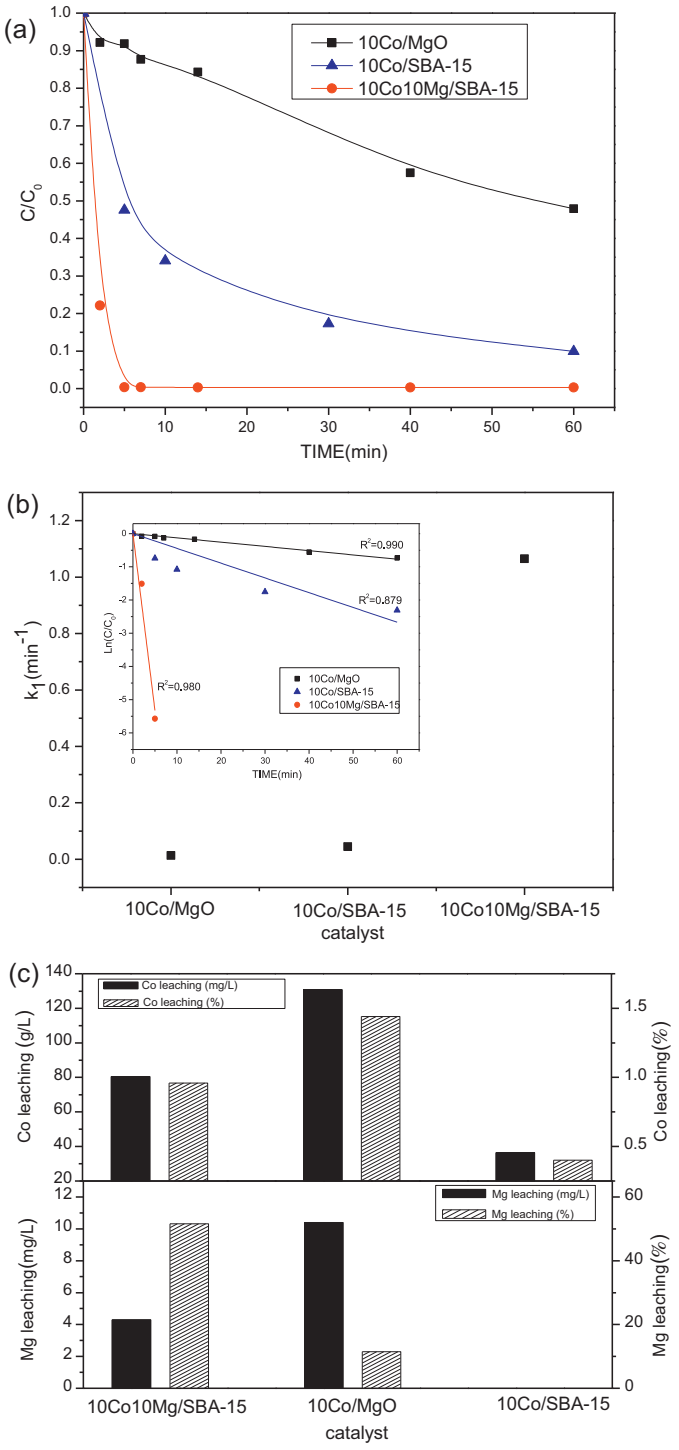

Fig. 10. Performance of cobalt-based heterogeneous catalysts with various supports ((a) RhB degradation, (b) RhB degradation kinetics, (c) cobalt and magnesium leaching, C_{Rh}: 5.0 mg/L, molar ratio of oxone/RhB: 10:1, catalyst dosage: 0.10 g/L, T: 25 °C, reaction time: 1 h, and no solution pH adjustment).

of Mg leaching for 10Co/MgO, but the Mg leaching percent was as high as 51% at the first application.

Fig. 11 also shows the contrast of RhB degradation in the presence of heterogeneous CoMg/SBA-15 or homogeneous Co(II) and oxone. In Fig. 11, RhB degradation in homogeneous Co(II)–oxone systems showed similar behavior, with the degradation efficiency increasing with increasing cobalt ion concentration and degradation rate keeping relatively slow in the process. The

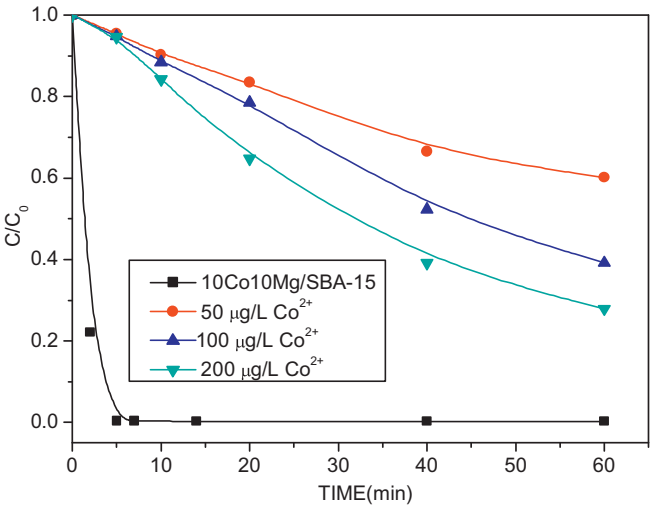

Fig. 11. RhB degradation in the presence of heterogeneous CoMg/SBA-15 or homogeneous Co(II) and oxone (C_{Rh}: 5.0 mg/L, molar ratio of oxone/RhB: 10:1, 10Co10Mg/SBA-15 dosage: 0.10 g/L, $C_{Co^{2+}}$: 50, 100, 200 μg/L, T: 25 °C, reaction time: 1 h, and no solution pH adjustment).

degradation of RhB in 60 min enhanced from 39 to 72% when cobalt ion concentration increased from 50 to 200 μg/L, indicating that 200 μg/L of cobalt ion concentration was not high enough to achieve the complete transformation of RhB. RhB degradation in 10Co10Mg/SBA-15–oxone system was much faster than those in homogeneous Co(II)–oxone systems, even though cobalt ion concentration was high up to 200 μg/L. For 10Co10Mg/SBA-15–oxone system, complete RhB decomposition could be achieved in about 5 min with Co leaching being 80 μg/L (0.96%). By a comparison with the data from the homogeneous Co(II)–oxone, it is believed that the heterogeneous 10Co10Mg/SBA-15 instead of the cobalt ions in solution was responsible for the catalytic degradation of RhB, i.e. the activation of oxone by 10Co10Mg/SBA-15 was through the heterogeneous pathway.

3.3.2. *Effect of Mg loadings on performance of catalyst CoMg/SBA-15*

The Mg loading on SBA-15 is supposed to be important to the catalyst performance. RhB degradation on CoMg/SBA-15 with various Mg loadings is presented in Fig. 12(a), and corresponding degradation kinetics is shown in Fig. 12(b). For the four CoMg/SBA-15 catalysts, the similar RhB degradation is observed regardless of the Mg loading in CoMg/SBA-15, with almost 100% RhB decolourization occurring within about 10 min (Fig. 12(a)). However, the Mg loading exerted a slight impact on the initial degradation rate of RhB. As seen in Fig. 12(b), the degradation rate constant of RhB for 10Co10Mg/SBA-15 is higher than any other catalyst. Furthermore, Co and Mg leachings after the utilization of CoMg/SBA-15 with various Mg loadings are shown in Fig. 12(c). Mg leaching concentration increased from about 2.5 mg/L to about 7 mg/L with increasing Mg loading from 5 to 20%, but the Mg leaching percent change little from 46 to 54%. On the other hand, Co leaching concentration first remarkably decreased from the maximum of 570 μg/L for 10Co5Mg/SBA-15 to the minimum of 80 μg/L for 10Co10Mg/SBA-15 and then slightly increased with increased Mg loading, and Co leaching percent first sharply decreased from 6.60% for 10Co5Mg/SBA-15 to 0.96% for 10Co10Mg/SBA-15, and then increased a little for 10Co15Mg/SBA-15 and 10Co20Mg/SBA-15. Mg is one of essential elements required by human body and is not a regulated element in aqueous environment. In this investigation, the Mg leaching concentrations were not more than 7 mg/L, i.e. the Mg level in the effluent could not exceed 7 mg/L, implying that

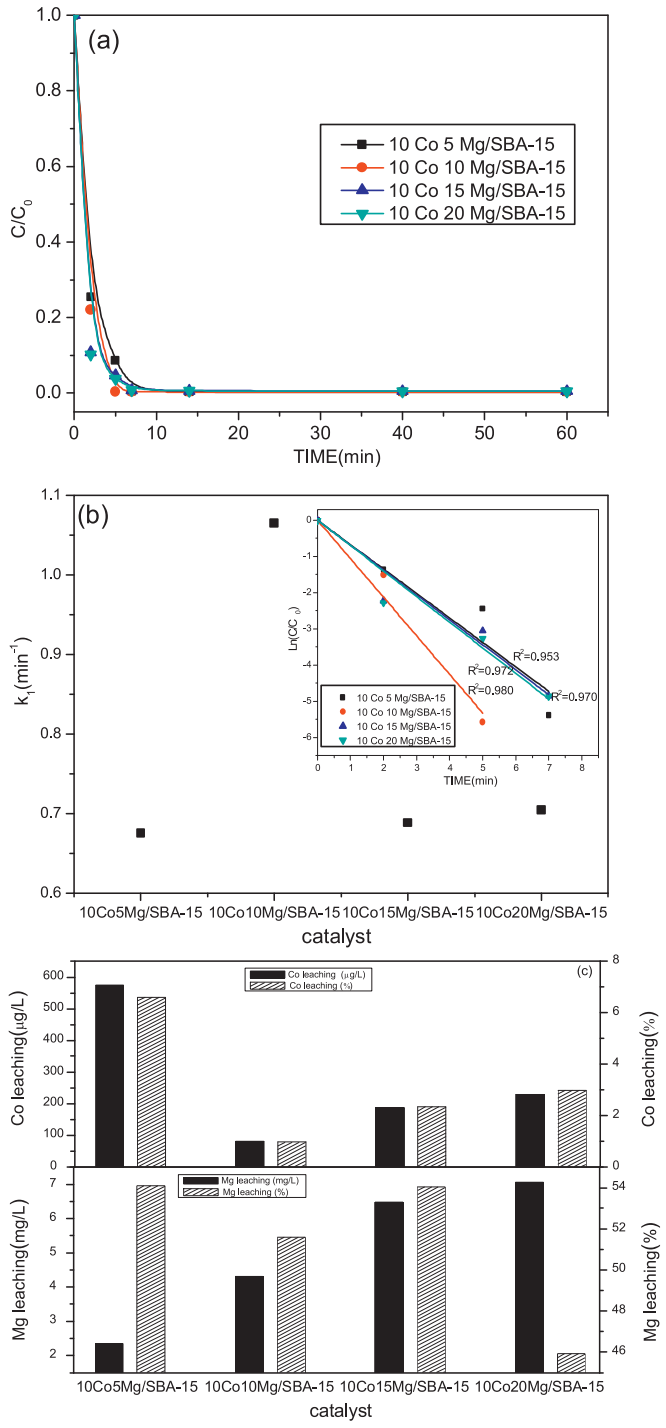

Fig. 12. Performance of CoMg/SBA-15 catalysts with various Mg loadings ((a) RhB degradation, (b) RhB degradation kinetics, (c) cobalt and magnesium leaching, C_{Rh} 5.0 mg/L, molar ratio of oxone/RhB: 10:1, 10Co10Mg/SBA-15 dosage: 0.10 g/L, T: 25 °C, reaction time: 1 h, and no solution pH adjustment).

the Mg loading on the CoMg/SBA-15 catalyst will not result in the extra environmental and health problems. Although Co element is one of regulated heavy metal elements, the minimum Co leaching of 80 μg/L (0.96%) from the 10Co10Mg/SBA-15 was comparable to the minimum leaching 36 μg/L (0.40%) from Co/SBA-15, attaining the acceptable level meeting the relevant environmental standard. In overview, the 10Co10Mg catalyst was selected as the best one among the four catalysts, and believed to be promising for practical application.

Table 2
Kinetic rate constants of organic degradation in the presence of Co supported catalyst/oxone.

Catalyst	Model compound	Rate constant (k_1, min^{-1})	R^2	Reference
Co/activated carbon	Phenol	0.125	0.991	[19]
Co/carbon-aerogel	Phenol	0.0289	0.992	[20]
Co/carbon-xerogel	Phenol	0.0916	0.982	[21]
$CoFe_2O_4$/graphene oxide	Phenol	0.1001	0.982	[22]
Co/red mud	Phenol	0.0371	–	[27]
Co/fly ash	Phenol	0.00513	–	[27]
Co/mesoporous MnO_2	Phenol	0.0425	0.996	[30]
Co/resin	Monuron (herbicide)	0.110	0.950	[26]
Co/SBA-15	Rhodamine B	0.063	0.971	This work
CoMg/SBA-15	Rhodamine B	1.065	0.980	This work
Co/MgO	Rhodamine B	0.013	0.990	This work

For heterogeneous Co catalysts with oxone, few investigations have reported the kinetics of organic degradation. The kinetics changed with different reaction conditions. Wang's research team have investigated the kinetics of heterogeneous activation of oxone with various cobalt supported catalysts for phenol degradation, and found that the degradation followed the first order or zero order kinetics, depending on the specific systems of catalyst–oxone–organics [17–22,25,27,29,30]. Among them, Co/SiO_2 [17,18], Co/TiO_2 [18], Co/Al_2O_3 [18], Co/zeolite [25], and Co/SBA-15 [29] exhibited the zero order kinetics, which suggested that the generation of active sulphate radicals was the rate controlling step for phenol degradation and the phenol concentration in solution would not play a significant role due to the slow surface reaction between supported Co and oxone [17,18]. On the other hand, Co/activated carbon [19], Co/carbon-aerogel [20], Co/carbon-xerogel [21], $CoFe_2O_4$/graphene oxide [22], Co/red mud [27], Co/fly ash [27], and Co/mesoporous MnO_2 [30] presented the first order kinetics, which is due to strong adsorption of phenol on the supports [18]. Chu et al. [26] also found that the decomposition of Monuron (one herbicide) in the presence of Co/resin and oxone followed quite well the first-order kinetics. In our investigation, the degradation of Rhodamine B in the presence of CoMg/SBA-15, or Co/SBA-15, or Co/MgO with oxone was found to obey the first order kinetics well. Table 2 presents the existent reaction rate constants of organic degradation in the presence of Co supported catalyst/oxone. From Table 2, it was observed that CoMg/SBA-15 with oxone for the degradation of the refractory organic pollutant RhB has the highest reaction rate constant among the Co supported catalyst available.

3.3.3. *Mineralization and degradation mechanism of RhB in the CoMg/SBA-15 and oxone system*

Since the decomposition intermediates of some organic substances such as RhB can be more harmful than the original ones, the mineralization of RhB should be ensured before the effluent discharge. Moreover, the mineralization is capable of revealing the degree of oxidative destruction of organic pollutants such as dye RhB. Generally, the mineralization can be represented by the TOC removal of organic compound solutions. The TOC in the present RhB solutions can be calculated stoichiometrically and theoretically by the following equation: $C_{28}H_{31}ClN_2O_3 + 73KHSO_5 \rightarrow 28CO_2 + 14H_2O + Cl^- + 2NO_3^- + 3H^+ + 73KHSO_4$. Fig. 13 shows the RhB mineralization profiles under different oxone dosages and reaction time in the presence of 10Co10Mg/SBA-15. As observed in Fig. 13, under the two different reaction time the RhB mineralization increases from approximately 15% for 10:1 of oxone/RhB ratio to about 75% for 30:1 of oxone/RhB ratio, suggesting that oxone dosage is more influential than the reaction time and the oxone dosage is less than the required

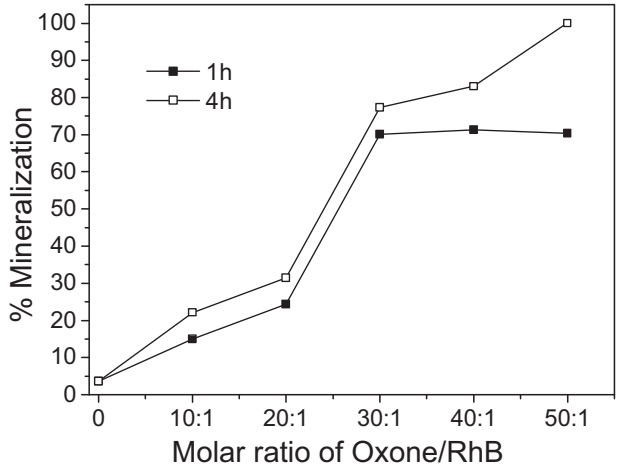

Fig. 13. RhB mineralization in the presence of 10Co10Mg/SBA-15 and oxone after 1 h and 4 h of reaction (C_{Rh}: 5.0 mg/L, molar ratio of oxone/RhB: 10:1, 20:1, 30:1, 40:1 and 50:1, 10Co10Mg/SBA-15 dosage: 0.10 g/L, T: 25 °C, reaction time: 1 h or 4 h, and no solution pH adjustment).

stoichiometric dosage for complete mineralization. However, the RhB mineralization for the oxone/RhB ratios more than 30:1 and 1 h reaction time kept unchanged due to the limited reaction time, and the mineralization for 4 h reaction time continually but slowly increased with increasing oxone/RhB ratio up to almost 100% at 50:1 of oxone/RhB ratio, indicating that the mineralization of RhB would be achieved under appropriate conditions and the degradation of the intermediates in the latter stage of reaction duration might be more difficult.

By a comparison, it could be found that there was a remarkable difference between the RhB degradation efficiency and its mineralization at 10:1 of molar ratio of oxone/RhB, indicating that the mineralization of RhB is much more difficult than its decolourization mainly due to the deficiency of the oxidant oxone in this case.

Fig. 14(a) shows the temporal evolution of spectral changes during the RhB degradation in the presence of the Co/SBA-15 catalyst and oxidant oxone. It is known that the RhB degradation occurs via two competitive processes: one is N-de-ethylation, and the other is the destruction of the conjugated structure [46,47]. As shown in Fig. 14(a), RhB shows a major absorption band at 552 nm, and there are blue shift of the main chromophore band at 552 nm of RhB and a gradual depletion of the absorbance peak, with no new bands appearing obviously. The blue shift might be ascribed to the intermediates of N-de-ethylation, the depletion of the RhB absorbance might be due to the destruction of the conjugated structure, and no new band occurrence eliminated the possibility of any complex formation originated from Co/SBA-15, oxone and RhB. Consequently, it can be derived that the destruction of the conjugated structure happened simultaneously with N-de-ethylation during the degradation of RhB with Co/SBA-15 catalyst and oxone.

The oxidation of RhB can either take place on the surface of catalysts after the adsorption of RhB molecules on Co/SBA-15 or in the solution after the desorption of the generated active sulphate radicals from the catalyst surface. Based on the previous investigations [3,16,48–51], the RhB degradation or mineralization in the presence of Co/SBA-15–oxone system can be supposed to occur as follows:

$$\text{MS-Co}^{2+} + \text{H}_2\text{O} \rightarrow \text{MS-CoOH}^{+} + \text{H}^{+}(\text{slow})(\text{MS–mesoporoussilica}) \quad (1)$$

$$\text{MS-CoOH}^{+} + \text{HSO}_5^{-} \rightarrow \text{MS-CoO}^{+} + \text{SO}_4^{\bullet -} + \text{H}_2\text{O} \quad (2)$$

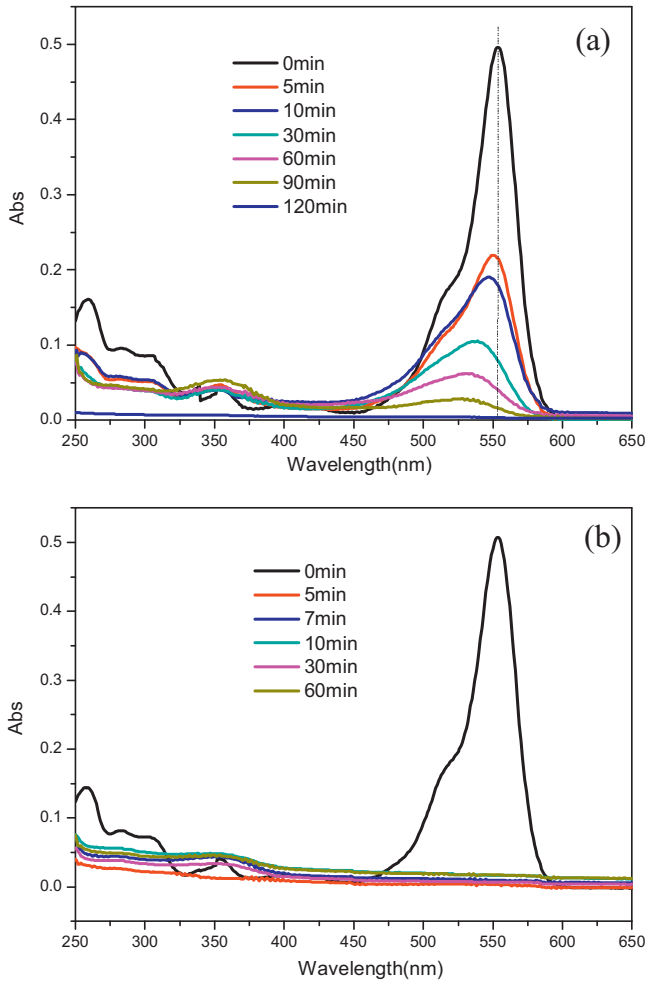

Fig. 14. UV–vis spectra of RhB degradation ((a) on 10Co/SBA-15, (b) on 10Co10Mg/SBA-15, C_{Rh}: 5.0 mg/L, molar ratio of oxone/RhB: 10:1, catalyst dosage: 0.10 g/L, T: 25 °C, reaction time: 1 h or 2 h, and no solution pH adjustment).

$$\text{SO}_4^{\bullet -} + \text{RhB}(\text{C}_{28}\text{H}_{31}\text{ClN}_2\text{O}_3) \rightarrow \text{RhB-SO}_4^{\bullet -} \rightarrow \text{severalsteps} \rightarrow \text{CO}_2 + \text{H}_2\text{O} + \text{SO}_4^{2-} + \text{NO}_3^{-} + \text{Cl}^{-} \quad (3)$$

The results of Fig. 14(a) emanate principally from an attack of the chromophoric structure as well as the ethyl groups of RhB by $SO_4^{\bullet -}$ radicals in the system of Co/SBA-15 and oxone. The rate-limiting step for MS-Co(II)-mediated oxone activation is the generation of MS-Co(II)–OH complexes derived from H_2O dissociation with MS-Co(II) (Eq. (1)) [12,16]. After loading Mg on support SBA-15, the resultant 10Co10Mg/SBA-15 has not only some primary property of Co/SBA-15 but also a much higher basicity than Co/SBA-15, thus possessing high content of surface hydroxyl groups. As a result, the formation of MS-Co(II)–OH species is greatly facilitated on the 10Co10Mg/SBA-15, thus favoring the sulphate radical generation. The UV–vis spectral changes observed during the degradation of RhB in the presence of 10Co10Mg/SBA-15 and oxone are depicted in Fig. 14(b). As shown, the absorption peak of the dye RhB diminishes very fast disappearing completely at 5 min of the reaction due to a great amount of sulphate radicals produced in this period, and there is no shift of the main chromophore band as well as no newly observed absorption peak. However, we would also propose that the degradation of RhB under the influence of CoMg/SBA-15 and oxone was attributed to both the destruction of the conjugated structure and the N-de-ethylation, yet the former was predominant [46]. Based on the

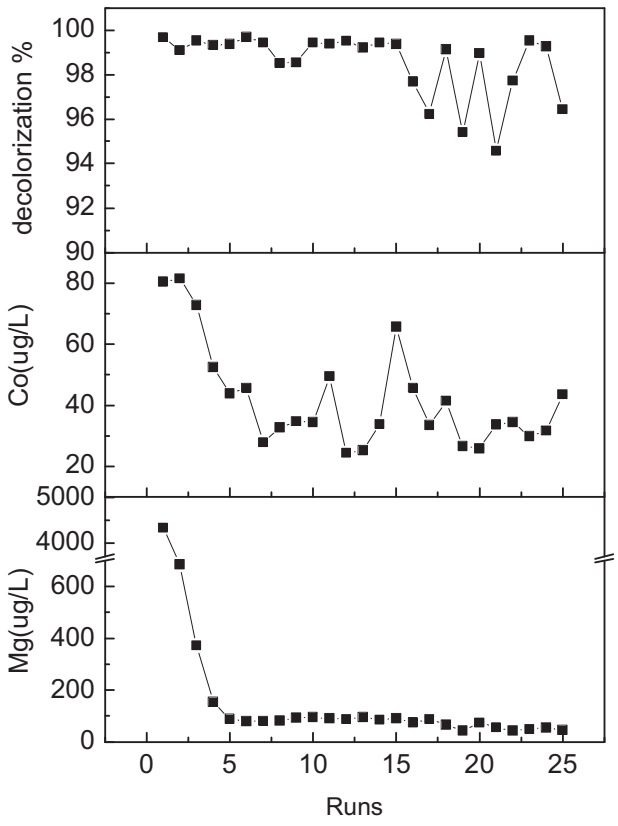

Fig. 15. Recycling performance of catalyst 10Co10Mg/SBA-15 (C_{Rh}: 5.0 mg/L, molar ratio of oxone/RhB: 10:1, 10Co10Mg/SBA-15 dosage: 0.10 g/L, *T*: 25 °C, reaction time: 1 h, and no solution pH adjustment).

degradation pathways, the following could be proposed about the degradation intermediates: in the early stage of degradation of RhB, the main intermediates are N,N-diethyl-N′-ethylrhodamine (DER), N,N-diethyl-rhodamine (DR), N-ethylrhodamine (ER), and rhodamine (R). As subsequent degradation of RhB takes place, these large molecular intermediates are further degraded into various small molecular alcohols and organic acids including butane-1,3-diol, phthalic acid, 3-nitrobenzoic acid, maleic acid, malonic acid, succinic acid, oxalic acid, etc. These organic acids and alcohols were finally mineralized to H_2O and CO_2 [47,52,53].

3.3.4. *Reusability of catalyst CoMg/SBA-15*

Owing to the extremely high activity of 10Co10Mg/SBA-15 in activation of oxone for the generation of sulphate radicals and the subsequent degradation of RhB, it is essential to evaluate the reusability of the spent catalyst. Fig. 15 shows the reuse performance of 10Co10Mg/SBA-15, represented by RhB decolourization, cobalt and magnesium leaching concentrations in solution during the 25 recycling runs.

As observed from the figure, the catalyst 10Co10Mg/SBA-15 kept the high activity during the 25 cycles, with a RhB degradation efficiency more than 94%. It was also observed that the cobalt leaching concentration ranged from the maximum of 80 μg/L for the initial two runs to the minimum of 25 μg/L, while the magnesium leaching concentration decreased from the maximum of 4.3 mg/L for the first run to less than 100 μg/L for the circles after circle 5. It was reported that the carbon deposit formed on the catalyst surface during the decomposition of organic compounds would occupy the active sites of the catalyst resulting in the decrease of its catalytic activity [54,55]. The unchanged high activity of the catalyst and acceptable Co and Mg leachings in the solution during the recycling test could be ascribed to the calcination at 400 °C of spent catalysts in the regeneration, which favoured the removal of the deposit on the catalyst surface and promoted the connection of Co and Mg with the support.

4. Conclusions

A modified heterogeneous cobalt catalyst CoMg/SBA-15 was synthesized through an incipient wetness impregnation technique using SBA-15 as the support and $Co(NO_3)_2{\cdot}6H_2O$ and $Mg(NO_3)_2{\cdot}6H_2O$ as the precursors, respectively. The CoMg/SBA-15 occurred as agglomerates of more than 0.3 μm in particle size, and Co and Mg species as Co_3O_4 and Mg oxide crystallites, respectively, were detected to be inside and outside the support pores with the diameter of about 6–7 nm. Mg oxides in CoMg/SBA-15 played an important role in the increase of dispersion of Co_3O_4 on the catalyst and the generation of basic sites on catalyst surface facilitating the formation of surface Co–OH complex which is vital for oxone activation. The Co/SBA-15–oxone–RhB system, as a test control, was proven to be effective for activation of oxone generating sulphate radicals for degrading RhB in solution, and the increase of Co/SBA-15 and oxone dosages enhanced the degradation efficiency and rate with a complete RhB degradation in 60 min and the Co leaching concentration less than 43 μg/L and the leaching percent less than 0.40% at appropriate Co/SBA-15 and oxone dosages. At the RhB concentrations investigated, RhB degradation, although a heterogeneous reaction, followed the first-order kinetics with respect to RhB. The CoMg/SBA-15 exhibited much higher activity than Co/SBA-15 and Co/MgO with the same Co loading on the catalysts in degrading RhB by sulphate radicals from oxone, with nearly complete RhB degradation, almost complete TOC removal and low Co leaching occurring. The CoMg/SBA-15 also exhibited stable performance during the recycling test. The superior performance of CoMg/SBA-15 could be ascribed to the mesoporous characteristic of the support and the modified surface property of the catalyst. The system of CoMg/SBA-15 and oxone could be regarded as a novel promising heterogeneous catalytic oxidation system for the persistent organic pollutants in water.

Acknowledgments

This study was partially supported by the Key Subject of Shanghai Municipality, P.R. China (Project No. S30109). The characterization of prepared samples was supported by the Analytical and Testing Center of Shanghai University, Shanghai, P.R.China.

References

[1] S. Malato, J. Blanco, C. Richter, B. Braun, M.I. Maldonado, Applied Catalysis B: Environmental 17 (1998) 347–351.
[2] E. Chamarro, A. Marco, S. Esplugas, Water Research 35 (2001) 1047–1051.
[3] G.P. Anipsitakis, D.D. Dionysiou, Environmental Science and Technology 37 (2003) 4790–4797.
[4] M. Cheng, W. Ma, J. Li, Y. Huang, J. Zhao, Environmental Science and Technology 38 (2004) 1569–1575.
[5] X.Y. Chen, J.W. Chen, X.L. Qiao, D.G. Wang, X.Y. Cai, Applied Catalysis B: Environmental 80 (2008) 116–121.
[6] P. Neta, R.E. Huie, A.B. Ross, Journal of Physical and Chemical Reference Data 17 (1988) 1027–1284.
[7] G.P. Anipsitakis, D.D. Dionysiou, Applied Catalysis B: Environmental 54 (2004) 155–163.
[8] G.P. Anipsitakis, D.D. Dionysiou, Environmental Science and Technology 38 (2004) 3705–3712.
[9] G.P. Anipsitakis, D.D. Dionysiou, M.A. Gonzalez, Environmental Science and Technology 40 (2006) 1000–1007.
[10] G.P. Anipsitakis, E. Stathatos, D.D. Dionysiou, Journal of Physical Chemistry B 109 (2005) 13052–13055.
[11] K.H. Chan, W. Chu, Water Research 43 (2009) 2513–2521.
[12] Q. Yang, H. Choi, S.R. Al-Abed, D.D. Dionysiou, Applied Catalysis B: Environmental 88 (2009) 462–469.
[13] Y. Ding, L. Zhu, A. Huang, X. Zhao, X. Zhang, H. Tang, Catalysis Science and Technology 2 (2012) 1977–1984.

[14] Q. Yang, H. Choi, D.D. Dionysiou, Applied Catalysis B: Environmental 74 (2007) 170–178.
[15] Q. Yang, H. Choi, Y. Chen, D.D. Dionysiou, Applied Catalysis B: Environmental 77 (2008) 300–307.
[16] W. Zhang, H.L. Tay, S.S. Lim, Y. Wang, Z. Zhong, R. Xu, Applied Catalysis B: Environmental 95 (2010) 93–99.
[17] P. Shukla, H. Sun, S. Wang, H. Sun, H.M. Ang, M.O. Tadé, Separation and Purification Technology 77 (2011) 230–236.
[18] H. Liang, Y.Y. Ting, H. Sun, H.M. Ang, M.O. Tadé, S. Wang, Journal of Colloid and Interface Science 372 (2012) 58–62.
[19] P.R. Shukla, S. Wang, H. Sun, H.M. Ang, M. Tadé, Applied Catalysis B: Environmental 100 (2010) 529–534.
[20] Y. Hardjono, H. Sun, H. Tian, C.E. Buckley, S. Wang, Chemical Engineering Journal 174 (2011) 376–382.
[21] H. Sun, H. Tian, Y. Hardjono, C.E. Buckley, S. Wang, Catalysis Today 186 (2012) 63–68.
[22] Y. Yao, Z. Yang, D. Zhang, W. Peng, H. Sun, S. Wang, Industrial and Engineering Chemistry Research 51 (2012) 6044–6051.
[23] P. Shi, R. Su, F. Wan, M. Zhu, D. Li, S. Xu, Applied Catalysis B: Environmental 123–124 (2012) 265–272.
[24] P. Shi, R. Su, S. Zhu, M. Zhu, D. Li, S. Xu, Journal of Hazardous Materials 229–230 (2012) 331–339.
[25] P. Shukla, S. Wang, K. Singh, H.M. Ang, M.O. Tadé, Applied Catalysis B 99 (2010) 163–169.
[26] W. Chu, W.K. Choy, C.Y. Kwan, Journal of Agricultural and Food Chemistry 55 (2007) 5708–5713.
[27] E. Saputra, S. Muhammad, H. Sun, H.M. Ang, M.O. Tadé, S. Wang, Catalysis Today 190 (2012) 68–72.
[28] L. Hu, X. Yang, S. Dang, Applied Catalysis B: Environmental 102 (2011) 19–26.
[29] H. Liang, H. Sun, A. Patel, P. Shukla, Z.H. Zhu, S. Wang, Applied Catalysis B: Environmental 127 (2012) 330–335.
[30] P. Shukla, H. Sun, S. Wang, H.M. Ang, M.O. Tadé, Catalysis Today 175 (2011) 380–385.
[31] D. Zhao, Q. Huo, J. Feng, B.F. Chmelka, G.D. Stucky, Journal of the American Chemical Society 120 (1998) 6024–6036.
[32] S. Jun, S.H. Joo, R. Ryoo, M. Kruk, M. Jaroniec, Z. Liu, T. Ohsuna, O. Terasaki, Journal of the American Chemical Society 122 (2000) 10712–10713.
[33] Y. Wang, W. Chu, Industrial and Engineering Chemistry Research 50 (2011) 8734–8741.
[34] H.M.H. Gad, A.A. El-Sayed, Journal of Hazardous Materials 168 (2009) 1070–1081.
[35] A. Martí nez-de la Cruz, U.M. García Pé rez, Materials Research Bulletin 45 (2010) 135–141.
[36] M. Asilturk, F. Sayilkan, S. Erdemoglu, M. Akarsu, H. Sayilkan, M. Erdemoglu, E. Arpac, Journal of Hazardous Materials 129 (2006) 164–170.
[37] M. Hou, L. Liao, W. Zhang, X. Tang, H. Wan, G. Yin, Chemosphere 83 (2011) 1279–1283.
[38] M.A. Behnajady, N. Modirshahla, S. Bavili Tabrizi, S. Molanee, Journal of Hazardous Materials 152 (2008) 381–386.
[39] S. Merouani, O. Hamdaoui, F. Saoudi, M. Chiha, Chemical Engineering Journal 158 (2010) 550–557.
[40] C. Bai, X. Xiong, W. Gong, D. Feng, M. Xian, Z. Ge, N. Xu, Desalination 278 (2011) 84–90.
[41] J. Li, X. Zhang, Z. Ai, F. Jia, L. Zhang, J. Lin, Journal of Physical Chemistry C 111 (2007) 6832–6836.
[42] L. Du, J. Wu, C. Hu, Electrochimica Acta 68 (2012) 69–73.
[43] B. Marler, U. Oberhagemann, S. Vortmann, H. Gies, Microporous Materials 6 (1996) 375–383.
[44] J.D.S. Lisboa, D.C.R.M. Santos, F.B. Passos, F.B. Noronha, Catalysis Today 101 (2005) 15–21.
[45] Z. Hou, O. Yokota, T. Tanaka, T. Yashima, Applied Catalysis A: General 253 (2003) 381–387.
[46] T. Wu, G. Liu, J. Zhao, Journal of Physical Chemistry B 102 (1998) 5845–5851.
[47] Z. He, S. Yang, Y. Ju, C. Sun, Journal of Environmental Sciences 21 (2009) 268–272.
[48] J. Kim, J.O. Edwards, Inorganica Chimica Acta 235 (1995) 9–13.
[49] J.G. Muller, P. Zheng, S.E. Rokita, C.J. Burrows, Journal of the American Chemical Society 118 (1996) 2320–2325.
[50] Z.M. Zhang, J.O. Edwards, Inorganic Chemistry 31 (1992) 3514–3517.
[51] R.C. Thompson, Inorganic Chemistry 20 (1981) 1005–1010.
[52] X. Zhao, Y. Zhu, Environmental Science and Technology 40 (2006) 3367–3372.
[53] K. Yu, S. Yang, H. He, C. Sun, C. Gu, Y. Ju, Journal of Physical Chemistry A 113 (2009) 10024–10032.
[54] J.A. Melero, G. Calleja, F. Martínez, R. Molina, M.I. Pariente, Chemical Engineering Journal 131 (2007) 245–256.
[55] J.H. Ramirez, F.J. Maldonado-Hódar, A.F. Pérez-Cadenas, C. Moreno-Castilla, C.A. Costa, L.M. Madeira, Applied Catalysis B: Environmental 75 (2007) 312–323.